Journal of Materials Chemistry

Cite this: *J. Mater. Chem.*, 2011, **21**, 80

www.rsc.org/materials

PAPER

Direct evidence of ZnO morphology modification *via* the selective adsorption of ZnO-binding peptides†

Mei-Keat Liang, Olivier Deschaume,‡ Siddharth V. Patwardhan§ and Carole C. Perry*

Received 5th July 2010, Accepted 27th September 2010
DOI: 10.1039/c0jm02124e

Biomolecule-mediated ZnO synthesis has great potential for the tailoring of ZnO morphology for specific application in biosensors, window materials for display and solar cells, dye-sensitized solar cells (DSSCs), biomedical materials, and photocatalysts due to its specificity and multi-functionality. In this contribution, the effect of a ZnO-binding peptide (ZnO-BP, G-12: GLHVMHKVAPPR) and its GGGC-tagged derivative (GT-16: GLHVMHKVAPPRGGGC) on the growth of ZnO crystals expressing morphologies dependent on the relative growth rates of (0001) and (10$\bar{1}$0) planes of ZnO have been studied. The amount of peptide adsorbed was determined by a depletion method using oriented ZnO films grown by Atomic Layer Deposition (ALD), while the adsorption behavior of G-12 and GT-16 was investigated using XPS and a computational approach. Direct evidence was obtained to show that (i) both the ZnO-BP identified by phage display and its GGGC derivative (GT-16) are able to bind to ZnO and modify crystal growth in a molecule and concentration dependent fashion, (ii) plane selectivity for interaction with the (0001) *versus* the (10$\bar{1}$0) crystal planes is greater for GT-16 than G-12; and (iii) specific peptide residues interact with the crystal surface albeit in the presence of charge compensating anions. To our knowledge, this is the first study to provide unambiguous and direct quantitative experimental evidence of the modification of ZnO morphology *via* (selective and non-selective) adsorption–growth inhibition mechanisms mediated by a ZnO-BP identified from phage display libraries.

Introduction

The realization of the ZnO era in the electronics and optoelectronics industries may be possible if the excellent electrical and optical properties of ZnO,[1–3] from sub-nanometre quantum dots to micrometre sized crystals, can be exploited. The challenges ahead can be generally classified into four areas: crystallinity and purity of ZnO; doping effectiveness and efficiency; size, morphology and functional structure assembly; and, last but not least, process feasibility and economics. Among these, morphology control has been given much attention since the successful application of ZnO in many instances relies on its shape- and size-dependent properties.[2] Highly crystalline ZnO crystals with diverse nanostructures, from simple to hierarchical, have been produced by vapor route synthesis.[1,2,4–12] However, the solution route offers a simpler, low cost scale-up, "green", and versatile alternative for ZnO synthesis.

The morphology of ZnO synthesized in solution (aqueous and non-aqueous) can be tuned *via* three distinct approaches: (i) the use of structure-directing agents (SDAs); (ii) the retention of ZnO precursor structures, such as layered basic zinc salt (LBZS), with ZnO formation realized by thermal decomposition; and (iii) a localized-reaction approach such as sonochemical and microwave-assisted synthesis. The most commonly used approach is that involving SDAs ranging from simple molecules, such as amines[13–16] and anionic species,[17–21] to polymers (DBCP,[22–29] PVP,[30–42] PAM,[29] and PAH[43]) and biomolecules.[44–52] The SDAs have been shown to affect the morphology of ZnO by imposition of effects on nucleation and/or growth of the crystals. Among these SDAs, biomolecules have received little attention in ZnO synthesis because of their complexity, high cost, and sensitivity to reaction conditions. Nonetheless, the use of biomolecules to direct ZnO synthesis is attractive for a number of reasons. The first is the potential of biomolecules to direct ZnO formation

Biomolecular and Materials Interface Research Group, School of Science and Technology, Nottingham Trent University, Clifton Lane, Nottingham, NG11 8NS, UK. E-mail: Carole.Perry@ntu.ac.uk

† Electronic supplementary information (ESI) available: FTIR spectra, XRD diffractograms, and TGA curves for ZnO precipitates formed; Zn^{2+} (%) reacted as a function of reaction time for reactions in the presence of peptide; crystal orientation of ALD-grown ZnO films; pK_a values and structure of G-12 and GT-16 obtained using Marvin software; predicted adsorbing moieties of G-12 and GT-16 on (0001) and (10$\bar{1}$0) planes of ZnO, FTIR peak area analysis for nitrate ion amide bands, and the estimation of weight loss between 200 and 900 °C region due to NO_3^-. See DOI: 10.1039/c0jm02124e

‡ Present address: Unité POLY, Université Catholique de Louvain, Boltzmann A + 2, Croix du Sud, 1, B-1348, Louvain-la-Neuve, Belgium.
§ Present address: Department of Chemical and Process Engineering, University of Strathclyde, 75 Montrose St, Glasgow G1 1XJ, UK.

under mild reaction conditions.[53,54] Secondly, some biomolecule-directed syntheses have been shown to impose exquisite control on ZnO morphology/structure;[44–46,48,50,51,55] improve ZnO crystallinity;[50] template ZnO formation;[47,49,52,56] catalyze ZnO formation;[57,58] and also suppress ZnO formation.[44,45] These diverse effects can possibly be used to tune the morphology/structure-related properties of ZnO and thus its applications. Thirdly, biomolecules show remarkable recognition capabilities, functional specificity and multi-functional characteristics which may contribute to high efficiency and accuracy in ZnO structure tailoring. Finally, there is an infinite reservoir of biomolecules with highly diverse functionalities that can be explored and discovered.[53]

Some biomolecules have been shown to influence ZnO morphology. As an example, ZnO films have been formed on substrates in the presence of histidine and/or its dipeptides, however, when these biomolecules were absent, discrete ZnO microcrystals were obtained.[44,45] In another study, the change of reactant concentrations, including variation of histidine concentration, generated ZnO particles with diverse morphologies including microrods, flowers, and microshells.[48] ZnO microshells can also be produced by the use of cysteine[59] while the use of a urease enzyme has been shown to produce nanoshells with potentially tunable diameters.[47] The transformation of ZnO particles from spheres to hexagonal plates and ellipsoids has been achieved by progressive reduction of the chain length of silk fibroin added.[56] Hexagonal plates have also been synthesized using gelatine[50,51] and Arabic gum[55] from reactions where hexagonal pellets or irregularly shaped crystals were typically formed respectively. In addition, a three-dimensional interwoven mesoporous fibrillar ZnO structure has been obtained using eggshell membrane as a template.[49,52] With the exception of studies involving amino acids and dipeptides, biomolecules that have been used in the study of ZnO formation are mainly complex macromolecules and, in some cases, their reactivity is determined by their multiple active sites and secondary/tertiary conformations. Thus many of the "wonders" that occur in their presence are created in a "black box".

An alternative approach for the rational design of simpler biomolecules for the generation of materials with novel form and for the study of biomolecule-mediated interactions is application of the combinatorial display method where short peptides (7-mer or 12-mer) that have affinity towards the surface of a metal or metal oxide can be identified. Although there are limitations to this approach,[60,61] a number of metal-binding peptides (M-BPs)[62–65] and metal oxide-binding peptides (MO-BPs)[46,58,66–70] have been identified that have either been shown to have an affinity for the surface they were isolated from or have been shown to influence the growth of their respective metal or metal oxide. The identification of ZnO-binding peptides (ZnO-BPs) and understanding how they adhere to the surface of ZnO is potentially useful for the construction of artificial biomaterials, medical implants, and biosensors where biocompatibility is required. Peptides could also be used to control crystal growth, for example, producing ZnO with high surface to volume ratio for applications as solar cells, catalysts and sensors.[1–3,71]

Application of the combinatorial phage display method identified a ZnO-BP, EAHVMHKVAPRP (EM-12) and its GGGSC derivative, EAHVMHKVAPRP–GGGSC was found to catalyze ZnO formation from a stable $Zn(OH)_2$ sol.[58] This EM12–GGGSC peptide derivative was further attached to a genetically modified collagen-like triple helix template to generate ZnO nanowires.[72] EM-12 has also been used to assist in the immobilization of green fluorescent protein (GFP) on ZnO surfaces with a 15 amino acid linker (GGGSAGSAASGSGEF) being used to tether the protein to the ZnO-BP.[73] The interaction between the EM-12 peptide and the ZnO surface has been shown to occur *via* electrostatic interaction with the single lysine present in the peptide contributing significantly and surrounding non-charged residues also being influential. Others have isolated a ZnO-BP with 67% sequence similarity to EM-12, GLHVMHKVAPPR (G-12).[46] The authors have shown that a transformation of ZnO from bipyramidal hexagonal rods to hexagonal plates occurs when the concentration of a GGGC tagged derivative of G-12, GLHVMHKVAPRP–GGGC (GT-16) in a zinc nitrate–hexamethylenetetramine ($Zn(NO_3)_2$–HMTA) reaction system is increased.[46] The authors propose that GT-16 inhibited the growth of ZnO along its *c*-axis by selectively adsorbing on the (0001) plane of ZnO based on three pieces of indirect evidence: (i) the GT-16 concentration dependent reduction of the aspect ratio of ZnO, (ii) the (0001) plane of ZnO crystal was flat and well-defined, and (iii) addition of GT-16 to the reaction had no effect on the diameter of ZnO.

Hitherto, evidence for the ability of biomolecules to tune ZnO morphology has been gained for single amino acids,[44,45,48,59] short peptides,[44,45,46,58] through to complex macromolecules such as proteins.[47,50,51,57,72,74] However, the focus of research in this area has been generally application-driven, and a mechanistic understanding of biomolecule-mediated ZnO formation remains incomplete. It has been postulated widely that the suppression of ZnO growth along its *c*-axis by biomolecules (also by many synthetic polymers/molecules) may be due to the adsorption of growth-inhibiting additives on the (0001) plane of ZnO *via* electrostatic interactions[13,18–20,46,50,75] or growth-promoting additives on complementary planes[21,76,77] but no direct measurement of the interactions has been made.

Recently a theory of competitive adsorption–nucleation to explain changes of ZnO aspect ratio in the presence of polypeptides has been developed.[78] According to this theory, the adsorption of polypeptides on the (0001) plane of ZnO would reduce the surface energy of the plane which in turn reduces the aspect ratio of ZnO crystals formed. The calculated aspect ratio-to-polypeptide concentration relationship fitted extremely well with the experimental data from Tomczak *et al.*[46] However, direct empirical evidence has not been provided to support biomolecule (that when present have altered ZnO morphology) adsorption on crystal plane(s) of ZnO. The interaction of specific amino acids such as lysine and alanine with ZnO single crystal planes has been studied,[79,80] but their effect on ZnO morphology/growth has not yet been identified.[45] As other examples, the interaction of tryptophan,[81] bovine serum albumin,[82] and plasma proteins[83] with ZnO has also been studied experimentally using ZnO nanoparticles mainly characterized in terms of size,[81,83] shape,[81,83] and ζ potential.[83] Crystallographic information relating to the surfaces of these nanoparticles exposed to biomolecules was not provided.

In this study, we sought to obtain direct evidence for the selective adsorption of a ZnO-BP (G-12) and its GGGC tagged derivative (GT-16) on specific ZnO crystal plane(s) and related

these data to changes in crystal morphology. The experiments and molecular dynamics simulations were designed to provide direct evidence and provide answers to the following questions: (i) are the G-12 and GT-16 peptides able to bind to ZnO and/or modify crystal growth? (ii) is peptide binding dependent on ZnO crystal-plane and peptide-sequence? (iii) can we elucidate the molecular level interactions between peptide and ZnO?

Materials and methods

Zinc nitrate hexahydrate ($Zn(NO_3)_2 \cdot 6H_2O$), hexamethylenetetramine (HMTA, $C_6H_{12}N_4$), sodium monophosphate (NaH_2PO_4), sodium phosphate dibasic (Na_2HPO_4), sodium chloride (NaCl), trifluoroacetic acid (TFA, $C_2HF_3O_2$), thioanisole (C_7H_8S), 3,6-dioxa-1,8-octanedithiol (DODT, $C_6H_{14}O_2S_2$), 1 M hydrochloric acid (HCl), and a zinc atomic absorption standard solution (1000 ppm) were purchased from Sigma-Aldrich; diethyl ether was purchased from Fisher Scientific; *O*-benzotriazole-*N*,*N*,*N*′,*N*′-tetramethyl-uronium-hexafluoro-phosphate (HBTU) and all Fmoc-protected amino acids required for peptide synthesis were purchased from CEM Corporation while the arginine- and cysteine-preloaded Wang resins were obtained from Novabiochem®. All chemicals were used without further treatment. Distilled, deionized water (ddH_2O) with conductivity less than 1 μS cm^{-1} was used in all experiments.

Solid phase peptide synthesis

G-12 and GT-16 were prepared by solid phase methods using a microwave-assisted solid phase peptide synthesizer (CEM Corporation) *via* Fmoc chemistry.[84] Wang resins were used as the solid support. The following side chain protections were used: Pbf for arginine; Trt for cysteine and histidine; and Boc for lysine. The couplings, *via* a *O*-benzotriazole-*N*,*N*,*N*′,*N*′-tetramethyl-uronium-hexafluoro-phosphate (HBTU) condensation agent, were single except for arginine where a double coupling was used. The cleavage of the peptide from the resin and the deprotection of side chains were achieved in one step by treating the peptide resin with cleaving agent containing trifluoroacetic acid, thioanisole, ddH_2O, and 3,6-dioxa-1,8-octanedithiol (DODT). The cleaved peptides were re-precipitated in chilled diethyl ether, washed three times with the same solvent prior to lyophilisation at −70 °C using a Virtis-110 freeze-dryer. The purity of the lyophilized peptides was analyzed with a Dionex HPLC equipped with a UV detector (set at 214 nm) and a Jupiter 4u Proteo 90A C12 Reverse Phase column (Phenomenex). The purity of G-12 and GT-16 was determined as 95% and 88% respectively. The molecular weight (M_w) of the peptides was measured using a Bruker UltraflexIII TOF/TOF mass spectrometer and analyzed with Daltonics flexAnalysis software. The M_w of the peptides was confirmed to be on target where the calculated M_w for G-12 and GT-16 were 1341.6 g mol^{-1} and 1615.9 g mol^{-1} respectively while their measured M_w were 1341.7 g mol^{-1} and 1615.8 g mol^{-1} respectively.

ZnO synthesis and kinetic studies

100 mM $Zn(NO_3)_2 \cdot 6H_2O$, 100 mM HMTA, 30 mM G-12, and 30 mM GT-16 were prepared as stock solutions for this study. Prior to each reaction, equal volumes of the $Zn(NO_3)_2 \cdot 6H_2O$ and HMTA stock solutions were mixed and predetermined volumes of G12 or GT-16 stock solutions were added immediately to obtain final G-12 concentration or GT-16 concentration of 0 mM, 0.03 mM, 0.15 mM and 0.30 mM, respectively. The pH of the final solutions prepared was pH 6.9 ± 0.1 regardless of the presence of additives. Prepared solutions were incubated at 20 °C (24 hours ± 1 min) followed by immersion in a 65 °C water bath (72 hours ± 1 min). During the course of reaction, samples were taken at selected times (±1 min). The control reaction was performed in triplicate in a single run. Collected samples were centrifuged at 13 000 rpm for 3 minutes to separate any precipitate from the supernatant. The supernatant obtained was re-centrifuged using the same conditions before being sampled into acidified water for the determination of Zn^{2+} concentration, $[Zn^{2+}]$, using ICP-OES (Perkin Elmer Optima 2100DV). The precipitates were washed three times thoroughly with ddH_2O. Cleaned precipitates were lyophilized at −70 °C using a Virtis-110 freeze-dryer.

Characterization of lyophilized ZnO precipitates

The wurtzite phase of ZnO was confirmed using XRD (PANalytical X'Pert PRO, CuK_α radiation with wavelength of 1.54056 Å). Ground samples (if necessary) packed into an aluminium sample holder were scanned for 2θ from 5° to 70° at 45 kV accelerating voltage, 40 mA filament current, using a scan speed of 0.02° s^{-1} at room temperature. Diffraction patterns were analyzed using X'Pert-HighScore Plus (version 2.0a) program for diffractogram manipulation, background determination and peak identification. The morphology and size of the ZnO crystals of selected precipitates were studied using SEM (JEOL JSM-840A, 20 kV, gold sputter-coated samples). For size analysis, at least 50 crystals were studied and the aspect ratio (L/D = length/average diameter) of each individual crystal was determined. FTIR (Nicolet Magna IR-750, 256 scans, 2 cm^{-1} resolution) was used to detect ZnO, peptides, and any incorporated species in the precipitates with a pure KBr disk being used for the background. The amount of non-ZnO component (peptide) in the precipitates was determined by TGA (Mettler Toledo TGA/SDTA 851ᵉ) where samples were heated at 10° min^{-1} from 30 °C to 900 °C in air to ensure complete combustion of all organic material.

Peptide adsorption studies

The selective adsorption of G-12 and GT-16 on the (0001) and $(10\bar{1}0)$ planes of ZnO was studied at 25 °C using oriented ZnO films (~9 cm^2) grown on silicon wafers by the ALD technique. This temperature was chosen to minimize any change of peptide concentration during the experiment arising from experimental factors (only small film sizes could be prepared by ALD such that the concentration of zinc in solution was necessarily very low) other than direct binding. The crystal orientation of ZnO films is controlled by its deposition temperature: 280 °C and 165 °C being used for the (0001) and $(10\bar{1}0)$ planes respectively.[85] The as-grown ZnO films were annealed at 800 °C (1 hour) prior to the confirmation of crystal orientation by XRD. All substrates studied, ZnO films, silicon wafers, and glass slide, were cleaned with acetone, dried in air, and placed into 12 mL peptide solution

prepared in PBS (phosphate buffered saline, 50 mM phosphate and 150 mM NaCl, pH 7.0). Given the calculated planar Zn atom density on (0001) and (10$\bar{1}$0) planes of ZnO crystals are 10.94 atoms per nm^2 and 5.91 atoms per nm^2 respectively,[86] the number of peptide molecules added were 5 times the estimated number of Zn atoms present on the ZnO films (peptide-to-Zn ratio = 5). At predetermined incubation times (t = 0, 5 hours), aliquots were sampled from the peptide solution and assayed using the Micro-BCA (Bicinchoninic acid) method for peptide concentration (Thermo Fisher Scientific). The absorbance of aliquots from the assays was measured at 562 nm using a Unicam UV2 UV-VIS spectrometer and compared against a series of calibration peptide solutions (0–10.5 μM), prepared in the same medium. Adsorption tests were performed in independent triplicates. At the end of the adsorption test, ZnO films were cleaned with ddH_2O and air-dried at room temperature before being analyzed by XPS using a Kratos AXIS ULTRA with a monochromated Al-K_α X-ray source (1486.6 eV) operated at a 10 mA emission current and 10 kV anode potential (100 W). The pressure of the analysis chamber was 3×10^{-9} torr. A wide scan (10 minutes) and high resolution scans (10, 5, 20 and 5 minutes for Zn, O, N, and C respectively) were performed on each sample where the latter was charge-corrected to the hydrocarbon C1s peak (285 eV) and then quantified to compare the amounts of the relevant elements present using Kratos sensitivity factors. The pass energies for the wide scan and the high resolution scan were 80 eV and 20 eV respectively. Fresh ZnO films (not exposed to peptide solution), G-12, and GT-16 were also analyzed and used as references. Six areas were analyzed for the selected samples.

Computational calculations

A molecular dynamics (MD) simulation tool, GROMACS,[87] was used to computationally determine the stable configurations of G-12 and GT-16 in water. The energy of the peptides was minimized in explicit single point charge (SPC) water at 300 K with a time step of 2 fs and total simulation time of 2 ns using the OPLS-AA-(L)-all atom force field. Using the stable configurations obtained, the interactions of G-12 and GT-16 with the (0001) and (10$\bar{1}$0) planes of ZnO were studied in vacuum using the Materials Studio®4.3 Adsorption Locator module based on the Metropolis Monte Carlo algorithm.[88] The adsorption modes and adsorption energies of G-12 and GT-16 on these ZnO planes were studied and the adsorbing segments/moieties were identified.

Results and discussion

Understanding the anisotropic growth of ZnO in the absence of peptides

For comparison purposes, the ZnO-forming reaction used by Tomczak *et al.*[46] was adopted in this study. In brief, solutions of $Zn(NO_3)_2$–HMTA were incubated initially at 20 °C for 24 hours followed by raising the temperature of the reaction medium to 65 °C, where samples were taken and the progress of reaction monitored using analytical methods to measure the amount of Zn^{2+} remaining in solution, XRD to assess any crystalline phases present and SEM to analyse the morphology of the products. In the absence of the peptides, a gel-like intermediate compound

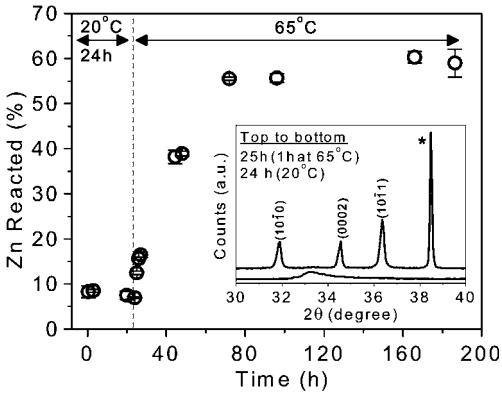

Fig. 1 The average and standard deviation (error bar) of Zn^{2+} consumed (in %) with time in the absence of additives (n = 3). The inset shows the diffraction peaks from precipitates collected after 24 hours ($t_{20\ °C}$ = 24 h) and 25 hours ($t_{20\ °C}$ = 24 h, $t_{65\ °C}$ = 1 h). The diffraction peak marked with an asterisk arises from the aluminium sample holder.

was formed at 20 °C, which was found to be neither ZnO nor pure $Zn(NO_3)_2 \cdot 6H_2O$ (ESI, Fig. S1†). ZnO was first detected by XRD at 1 hour (first sampling at 65 °C) after the reaction temperature was increased to 65 °C ($t_{20\ °C}$ = 24 h, $t_{65\ °C}$ = 1 h), Fig. 1 inset. The diffraction peaks obtained can be indexed to the hexagonal wurtzite structure of ZnO (JCPDS card no. 36-1451). At 65 °C, the amount of Zn^{2+} consumed for ZnO formation steadily increased from the stable level of ~10% at 20 °C until an equilibrium state was reached when ~60% of Zn^{2+} was reacted, Fig. 1. The non-ZnO gel-like precipitates collected after 24 hours ($t_{20\ °C}$ = 24 h) appeared to be continuous sheets with rough surfaces (Fig. 2a) as opposed to hexagonal ZnO crystals obtained at 65 °C (Fig. 2b–d). The absence of a centre of inversion in the wurtzite structure is known to result in ZnO having inherent asymmetry along its c-axis.[1] In this study, the anisotropic growth of ZnO crystals was clearly observed through the increase of crystal aspect ratio (L/D ± standard error) from 2.7 ± 0.1 to

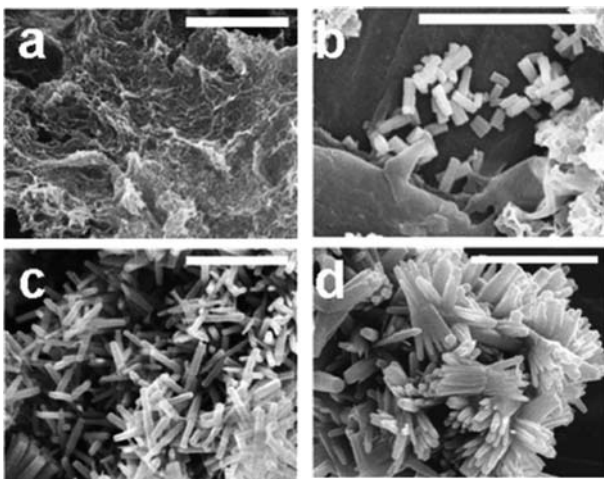

Fig. 2 SEM images for precipitates collected in the absence of additives after (a) 24 hours ($t_{20\ °C}$ = 24 h), (b) 25 hours ($t_{20\ °C}$ = 24 h, $t_{65\ °C}$ = 1 h), (c) 48 hours ($t_{20\ °C}$ = 24 h, $t_{65\ °C}$ = 24 h), and (d) 72 hours ($t_{20\ °C}$ = 24 h, $t_{65\ °C}$ = 48 h). Scale bars are 5 μm.

11.4 ± 0.2 for crystals collected after 25 hours ($t_{20\ ^\circ C}$ = 24 h, $t_{65\ ^\circ C}$ = 1 h, Fig. 2b) and 48 hours ($t_{20\ ^\circ C}$ = 24 h, $t_{65\ ^\circ C}$ = 24 h, Fig. 2c) respectively. Oriented attachment of ZnO rods along their *c*-axes was observed as the reaction was prolonged, Fig. 2d. This phenomenon, believed to be driven by surface energy reduction, has also been described in other publications, however, its cause is still debated.[39,76,89–93] Since ZnO was not detected at 20 °C, for simplicity, the reaction time is quoted as the reaction duration at 65 °C in all following sections, *i.e.* total reaction time of 25 hours and 48 hours are described as $t_{65\ ^\circ C}$ = 1 h and $t_{65\ ^\circ C}$ = 24 h respectively.

ZnO aspect ratio reduction by G-12 and GT-16

The addition of G-12 or GT-16 affected neither the Zn^{2+} consumption rate for ZnO formation nor the [Zn^{2+}] at equilibrium compared to the control reaction (ESI, Fig. S2†), suggesting that G-12 and GT-16 may not interact with Zn^{2+} species in solution. These data also suggest that the presence of these two peptides, for the concentration ranges used, does not affect nucleation. Similar to the control reactions, ZnO crystals were detected by XRD from precipitates collected at $t_{65\ ^\circ C}$ = 1 h, produced in the presence of G-12 and GT-16 (ESI, Fig. S3†). As anticipated, a reduction of crystal *L*/*D* as a function of peptide concentration was observed in the presence of GT-16 and G-12, Fig. 3. However, the effect was more prominent for GT-16 compared to G-12, Fig. 3a. This effect induced by G-12 and GT-16 started from the early stage of crystal growth ($t_{65\ ^\circ C}$ = 1 h)

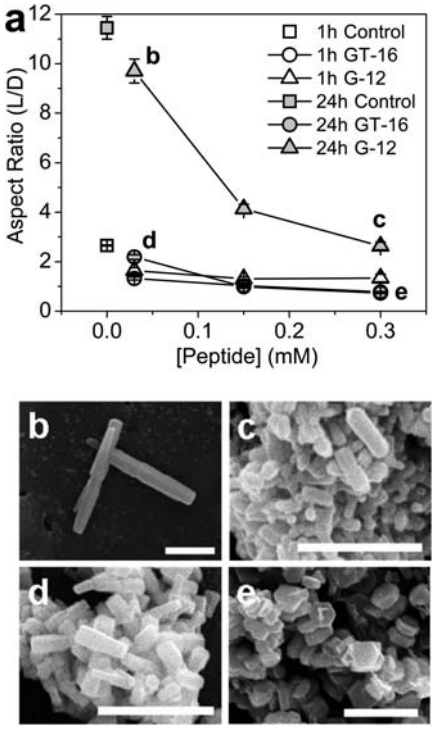

Fig. 3 (a) The average and 95% confidence interval of ZnO aspect ratio (*L*/*D*) as a function of peptide concentration, and SEM images of ZnO crystals formed after $t_{65\ ^\circ C}$ = 24 h in the presence of (b) 0.03 mM G-12, (c) 0.30 mM G-12, (d) 0.03 mM GT-16, and (e) 0.30 mM GT-16. Scale bars are 2 μm.

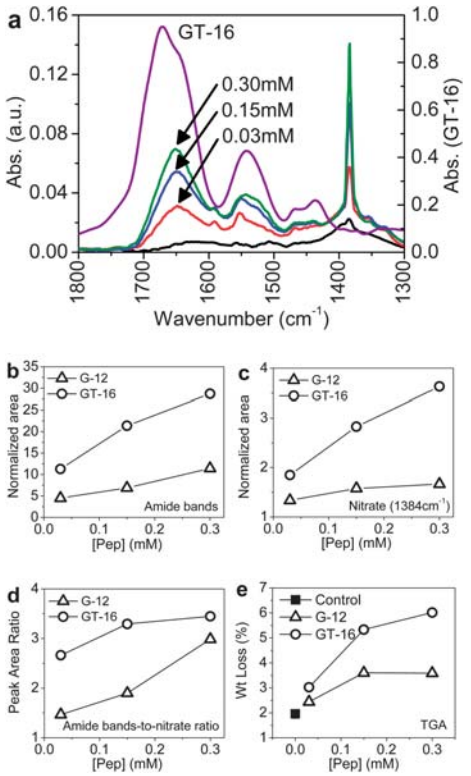

Fig. 4 The FTIR (a–d) and TGA (e) analyses of ZnO precipitates collected at $t_{65\ ^\circ C}$ = 24 h, produced in the presence of G-12 and GT-16. (a) The FTIR spectra of precipitates obtained in the presence of GT-16. The peak area ratio between samples (in the presence of peptides) and the control for peak area under (b) amide-I and amide-II bands (1480–1730 cm^{-1}), and (c) nitrate peak (1384 cm^{-1}). (d) The amide bands-to-nitrate peak area ratio within individual spectra as depicted in (a). (e) The weight loss attributed to the decomposition of the organic component (200–600 °C) where the error bar is the standard deviation for the control reactions (0 mM peptide, n = 3).

where the *L*/*D* was 1.0–1.7 compared to 2.7 for the control. Compared to the *L*/*D* reduction reported for GT-16,[46] the level of *L*/*D* reduction in this study was slightly higher at lower [GT-16] but these values converged as [GT-16] was increased.

ZnO precipitates ($t_{65\ ^\circ C}$ = 24 h) obtained in the presence of G-12 and GT-16 contain peptides as shown by the presence of the amide-I (1600–1700 cm^{-1}) and amide-II (1500–1600 cm^{-1}) bands in their FTIR spectra (Fig. 4a for GT-16 and ESI, Fig. S4† for G-12). The area under the two amide bands of these FTIR spectra was determined and normalized against the area under the control spectrum for the same frequency range. As shown in Fig. 4b, the amount of peptide incorporated in ZnO precipitates increased with the initial peptide concentration, supporting the coprecipitation of peptides with ZnO.

The presence of NO_3^- (1384 cm^{-1}, asymmetric stretch)[44,59,94,95] was also detected in all 48 hour precipitates including the control (Fig. 4a), and the gel-like intermediate compound produced after 24 hours ($t_{20\ ^\circ C}$ = 24 h) from the blank (ESI, Fig. S1†). The normalized area of the nitrate peak increased linearly as a function of peptide concentration, Fig. 4c, suggesting that NO_3^- ions may have formed a complex with, possibly, the cationic moieties of the peptide and co-precipitated with ZnO when peptides adsorbed on ZnO surfaces. A non-constant peak area ratio of the

amide-I and II bands to NO_3^- (1384 cm^{-1}) calculated from FTIR spectra suggests that not all cationic moieties of each peptide molecule have reacted with NO_3^-, Fig. 4d. It has been suggested that HMTA may adsorb on the (10$\bar{1}$0) plane of ZnO crystal,[92] however, this possibility can be discounted in this study based on the absence of the peak expected for adsorption of a tertiary amine (~1006 cm^{-1}) in all spectra including those from the control reaction (ESI, Fig. S4†).

The coprecipitation of peptides with ZnO was further supported by substantial weight loss for the ZnO samples prepared in the presence of peptides, with respect to the control reaction, monitored using TGA (ESI, Fig. S5†). The trend of organic component weight loss as a function of peptide concentration (Fig. 4e) was similar to the trend shown by FTIR results in Fig. 4b. The coprecipitation of NO_3^- with ZnO (suggested by FTIR results) did not alter the trend of the incorporated amount of peptide significantly (ESI, Fig. S6†). Therefore while reducing the aspect ratio of ZnO crystals, these two peptides co-precipitated onto/into the ZnO crystals. Furthermore, GT-16 which was incorporated to a greater extent than G-12, perhaps therefore has a stronger effect on L/D reduction compared to G-12. This may imply a correlation between the amount of peptide incorporated and the level of L/D reduction.

There were two observations which indirectly suggest peptide adsorption on ZnO surfaces. Firstly, a blue-shift of the amide-I band (from ZnO-peptide precipitates) relative to the amide-I band of the pure peptides was observed. The observed amide-I band shift of 20–26 cm^{-1} from 1671 cm^{-1} was likely to be due to the adsorption of peptides on crystal surfaces which alters the energy of vibration.[96] Secondly, a new peak at 1590–1594 cm^{-1}, assignable to the symmetric stretching of bound COO^- was detected.[40,97] Since both G-12 and GT-16 have no acidic amino acid residues, the bound COO^- most probably arose from the C-terminus of these peptides.

Modification of ZnO growth rate by G-12 and GT-16

In order to understand how ZnO growth has been affected and how the additional GGGC-tag of GT-16 enhanced the aspect ratio reduction, the growth rates of individual crystal dimensions from $t_{65\,^\circ C} = 1$ h to $t_{65\,^\circ C} = 24$ h were determined, namely, $\Delta L/\Delta t$ for length along the c-axis and $\Delta D/\Delta t$ for the average diameter along the a-axis, Fig. 5a and b.

In the absence of peptide, $\Delta L/\Delta t$ and $\Delta D/\Delta t$ for the ZnO crystals were 149 nm h^{-1} and 3.4 nm h^{-1} respectively. Addition of G-12 reduced $\Delta L/\Delta t$ gradually to ~10 nm h^{-1} as the peptide concentration was increased. In contrast, addition of GT-16, even at the lowest concentration (0.03 mg mL^{-1}), drastically reduced $\Delta L/\Delta t$ to ~7 nm h^{-1}, however, this growth rate was not affected by further increase in the peptide concentration. In the presence of GT-16, reduction in growth along the c-axis was compensated for by an increase in $\Delta D/\Delta t$. This contrasted with the crystal growth observed in the presence of G-12, where the average diameter of the ZnO crystals remained unchanged ($\Delta D/\Delta t \approx 0$) for the 23 hour analysis period regardless of the concentration of G-12 showing that G-12 has little or no influence on the a-axis growth of the crystal. The effect of increasing G-12 and GT-16 concentrations on the length and diameter growth of ZnO crystals from $t_{65\,^\circ C} = 1$ h to $t_{65\,^\circ C} = 24$ h, as described above, is illustrated by a scaled schematic in Fig. 5c. In contrast to the data presented by Tomczak *et al.* in their study using GT-16 where the observed aspect ratio reduction was reported as being due to crystal length reduction, our studies have shown that by separately analyzing the effect of the two peptides (G-12 and GT-16) on both the length and diameter of the crystals formed, we have discovered that the reduction of the ZnO aspect ratio is a combination of the presence of G-12 or GT-16 on both the length (c-axis) and diameter (a-axis) growth of the ZnO crystals.

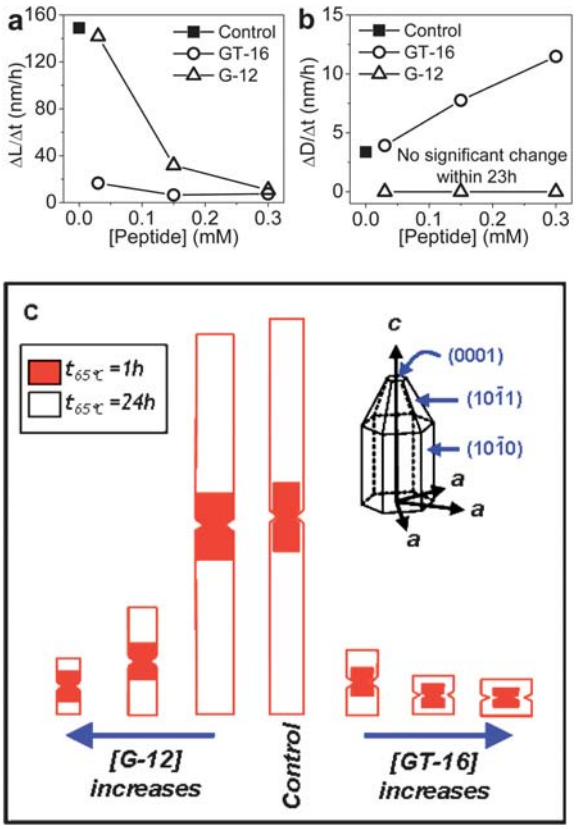

Fig. 5 The growth rate of (a) length, L, and (b) average diameter, D, of ZnO crystals within 23 hours of reaction at 65 °C, from $t_{65\,^\circ C} = 1$ h to $t_{65\,^\circ C} = 24$ h. (c) Schematic showing the effect of increasing G-12 and GT-16 concentrations on the length and diameter of ZnO crystals from $t_{65\,^\circ C} = 1$ h to $t_{65\,^\circ C} = 24$ h. The images of ZnO crystals are scaled.

Up to this point, the presence of G-12 and GT-16 has been confirmed to reduce the c-axis growth of ZnO crystals while the presence of G-12 has also retarded the diameter growth (a-axis) growth of the crystal. In addition, the coprecipitation of G-12 and GT-16 strongly correlated (quantitatively) with the reduction of crystal dimension growth rate. In many instances the presence of capping agents such as DBCP,[22–25] citrate ions,[19,20,75] hydroxyl ions,[13] *etc.* has been shown to reduce the aspect ratio of ZnO crystals. Since (0001) is a Zn-terminated plane, the capping agents that have reduced the aspect ratio of ZnO crystals and/or were proposed to adsorb on the (0001) plane are generally anionic or contain anionic moiety(ies). Therefore, based on this generally accepted rationalization, the inhibition of diameter growth in the presence of G-12 but not with GT-16 would lead to three possible speculations. Firstly, besides adsorbing on (0001),

G-12 molecules were able to adsorb onto the $(10\bar{1}0)$ plane of ZnO crystals, possibly *via* a different adsorption mechanism. Secondly, GT-16 selectively adsorbed onto the (0001) planes of ZnO crystals. Thirdly, the plane selectivity of GT-16 was attributable to the GGGC tag not present in G-12. To unravel the cause(s) of these interesting findings, the adsorption behavior of G-12 and GT-16 was studied.

A comparison of the adsorption of G-12 and GT-16 on ZnO crystal planes

The adsorption behavior of G-12 and GT-16 was studied by exposing ALD grown-ZnO films with either (0001) or $(10\bar{1}0)$ plane (ESI, Fig. S7†) to peptide solutions. The use of oriented-ZnO films eliminated any uncertainties of peptide adsorption sites, which may arise from the use of ZnO crystals with more than one surface crystallographic plane. The amount of peptide adsorbed and peptide density on the ZnO films were determined by a depletion method from the amount of peptide retained in solution after 5 hours of substrate exposure. From the amount adsorbed on the different substrates (area $\approx$ 9 cm^2), G-12 and GT-16 both showed material selectivity towards ZnO over silicon wafer and glass, Fig. 6a. Peptide density (Fig. 6b) was typically higher on the basal plane, ZnO(0001), compared to the side planes, Zn$(10\bar{1}0)$. The inter-plane density difference for GT-16 was 0.31 nmol cm^{-2} as compared to 0.08 nmol cm^{-2} for G-12, suggesting a preferential adsorption of GT-16 on the (0001) plane. Preferential adsorption of GT-16 supports the observation of reduced growth rate on the *c*-axis ($\Delta L/\Delta t$) but not on the *a*-axis ($\Delta D/\Delta t$) in its presence. The lower G-12 density on the (0001) plane and its weaker plane selectivity were demonstrated by the lower extent of ZnO aspect ratio reduction in its presence.

Evidence for peptide adsorption on ZnO crystal planes and the adsorption process being peptide- and crystal plane-dependent was provided by XPS analysis which confirmed that significant amounts of peptide were present on the ZnO films exposed to the solutions of the peptides, Fig. 7. The presence of peptide was confirmed *via* the detection of nitrogen (N 1s) with binding energy of ~400 eV. Fig. 7 shows the N 1s atomic % (high resolution scan) on exposed ZnO films, unexposed ZnO films, G-12, and also GT-16. XPS results obtained did not (quantitatively) coincide entirely with the adsorption results, inset of Fig. 7.

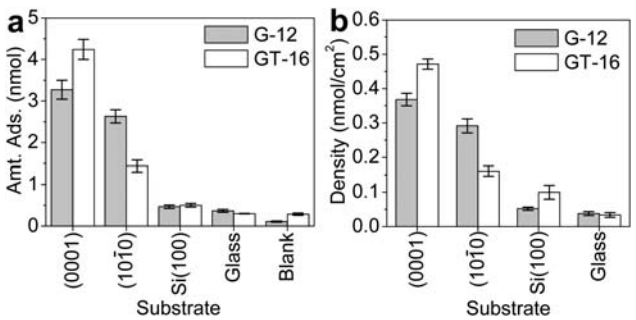

Fig. 6 The adsorption of G-12 and GT-16 on different substrates after 5 hours of exposure: (a) the amount adsorbed on a substrate with an area ~9 cm^2, and (b) peptide density. The error bars shown are the standard deviation ($n = 3$).

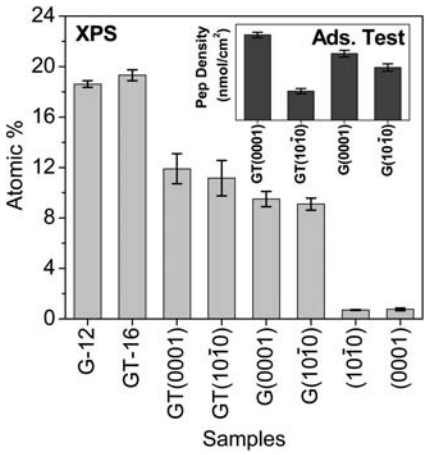

Fig. 7 The atomic % of N 1s determined using XPS (high resolution scan). GT and G denote GT-16 and G-12 respectively. Inset shows the peptide density on ZnO films reproduced from Fig. 6b.

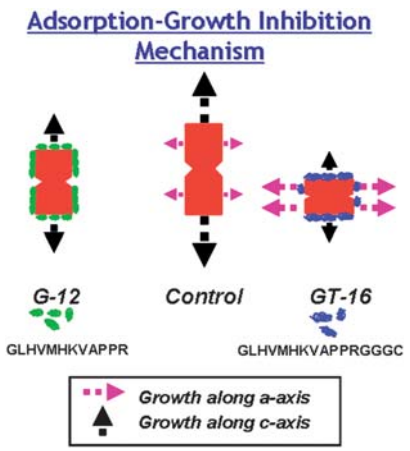

Scheme 1 The adsorption–growth-inhibition mechanism. The length and thickness of growth arrows reflects the growth rate of the crystals along their respective axes.

However, the important outcomes are summarized as follows: (i) the detection of a substantial amount of nitrogen on the surface of ZnO films (exposed to peptide solution) is direct evidence of peptide adsorption on ZnO crystal planes, (ii) the amount of G-12 adsorbed on the (0001) plane was slightly larger than on the $(10\bar{1}0)$ plane, which corroborated the experimental observations (Fig. 6b), and (iii) the amount of GT-16 adsorbed on the (0001) plane was significantly higher than G-12 on the same plane for both ZnO planes.

The presented data show that for ZnO formation in the presence of ZnO-BPs, both G-12 and GT-16 altered the growth rates of ZnO crystal planes and are adsorbed on these crystal planes, with the level of growth reduction being positively correlated with the amount of peptide adsorbed. Therefore the modification of ZnO crystal morphology by G-12 and GT-16 occurs *via* an adsorption–growth inhibition mechanism as illustrated in Scheme 1. Hitherto, the incorporation/adsorption of SDAs on ZnO has been shown qualitatively by FTIR, TGA,[21,23,34] fluorescence microscopy,[23,58] and SEM (through the presence and multiplication of growth spirals in the presence of

DBCPs).[25] To our knowledge, this is the first study providing unambiguous and direct quantitative experimental evidence, by the use of ALD-grown single orientation ZnO films, for the (selective and non-selective) adsorption-driven ZnO morphology modification by biomolecules and specifically a ZnO-BP identified from phage display libraries.

Adsorption and selective adsorption: cause and driving force

To complement the experimental data, a computational approach was employed to provide (calculated) energetic data and the prediction of binding moiety(ies). When exposed to ZnO surfaces in vacuum, the adsorption modes and adsorption energy (E_{ads}) of stable configurations of G-12 and GT-16 (simulated in water by MD) were determined. The adsorption of G-12 and GT-16 on ZnO planes was found to be an energetically favorable process, Fig. 8. The selective adsorption of GT-16 was self-explanatory based on a lower E_{ads} on the (0001) plane and a higher inter-plane E_{ads} of 288 kJ mol^{-1} as opposed to 100 kJ mol^{-1} for G-12. The low adsorption selectivity of G-12 can be attributed to competition in binding arising from the smaller difference in its inter-plane E_{ads}, thus an additional limitation of growth along the *a*-axis was observed.

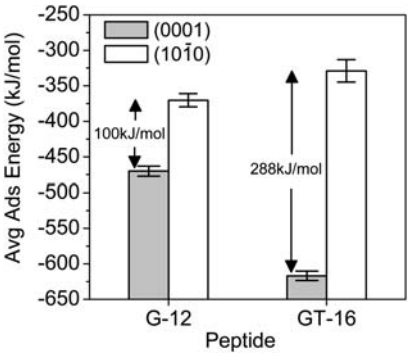

Fig. 8 The average adsorption energy and standard deviation of G-12 and GT-16 on (0001) and (10$\bar{1}$0) planes of ZnO. The standard deviation was less than 5% ($n = 10$).

Much literature has reported/proposed electrostatic interaction/coordination between the Zn^{2+} of the (0001) plane and additives (DBCP,[23,24,98] citrate,[19,20] phosphate,[17] TEA,[15,99] *etc.*) as being responsible for the adsorption of the specific additive on the (0001) plane. The charge and the extent of protonation/deprotonation of amino acid residues in G-12 and GT-16 at pH 6.9 $\pm$ 0.1 (based on their pK_a values, ESI, Fig. S8†) were determined, and compared with the predicted binding moieties (by simulation as shown in ESI, Fig. S9†) in Table 1.

As shown in Table 1, residues with cationic/neutral side chains were predicted to engage on the (0001) plane of ZnO, namely H_3 and K_7 for G-12, and G_1, H_6, and K_7 for GT-16. Since neutral imidazole nitrogen atoms could coordinate with Zn^{2+} using a lone pair on a nitrogen atom,[100] the prediction of H_3 (of G-12) and H_6 (of GT-16) binding on the (0001) plane of ZnO is not surprising. From the FTIR spectra of peptide adsorbed-ZnO precipitates, an absorption peak arising from the asymmetric stretching of NO_3^- (1384 cm^{-1}) was observed (Fig. 4a). The positive correlation between the amount of NO_3^- incorporated and the amount of peptide initially present (Fig. 4c) suggests that NO_3^- interacts with the cationic moieties of G-12 and GT-16. This interaction may reduce the repulsion between the peptide and Zn^{2+} ions on ZnO crystal planes and will be applicable for any positively charged amino acid residue present in the peptides. The prediction of cationic G_1 (of GT-16) and K_7 (of G-12 and GT-16) as favorable anchor points on the also cationic

Table 1 The prediction of bound amino acid residues of G-12 and GT-16 on ZnO surfaces[a,b]

	Plane	G_1	L_2	H_3	V_4	M_5	H_6	K_7	V_8	A_9	P_{10}	P_{11}	R_{12}	
	Side chain pK_a	—	—	6.92	—	—	6.08	10.21	—	—	—	—	6.53	
	Termini pK_a	7.41												3.33
G-12	(0001)			●				●						
G-12	(10$\bar{1}$0)			●				●						
	Protonation / Deprotonation of side chain	>50%		~50%			<50%	>50%					<50%	>50%[b]

	Plane	G_1	L_2	H_3	V_4	M_5	H_6	K_7	V_8	A_9	P_{10}	P_{11}	R_{12}	G_{13}	G_{14}	G_{15}	C_{16}	
	Side chain pK_a	—	—	7.09	—	—	6.24	10.21	—	—	—	—	6.69	—	—	—	10.05[b]	
	Termini pK_a	7.64																2.54
GT-16	(0001)	●					●	●										
GT-16	(10$\bar{1}$0)					●							●	●	●	●	●	
	Protonation / Deprotonation of side chain	~50%		~50%			<50%	>50%					<50%				>50%	>50%

[a] The side chain charge at pH 6.9 $\pm$ 0.1 (based on calculated pK_a): green cell for positive, white cell for neutral, and pink cell for negative. The side chain of a residue that binds on different ZnO planes (based on computational prediction): blue circles for (0001) plane and red circles for (10$\bar{1}$0) plane. [b] pK_b.

Zn-terminated (0001) plane was unexpected although the significance of K_7 in binding to ZnO surfaces has recently been shown by other experimentalists using the ZnO-BP EM12.[73] It is speculated that the R_{12} and C_{16} of G-12 and GT-16 respectively are able to bind to Zn^{2+} on the (0001) plane. The higher GT-16 density measured on the (0001) plane (adsorption test) may arise due to (i) higher binding capacity of H_6 (>50% neutral side chain) from GT-16 as opposed to ~50% neutral H_3 of G-12, and (ii) stronger binding of GT-16 through C_{16} *via* its C-terminal COO^- and its thiol sulfur which is able to bridge two Zn^{2+} ions.[101]

In comparison with peptide binding on the (0001) plane, the predicted binding residues on the $(10\bar{1}0)$ plane are very different for G-12 and GT-16. The predicted binding moieties from G-12 are polar (H_3 and K_7) but largely non-polar for GT-16 (M_5, R_{12}, and GGGC-tag). Due to the presence of both Zn^{2+} and O^{2-} on the $(10\bar{1}0)$ plane, cationic H_3 and K_7 are suggested to interact with O^{2-} *via* electrostatic interactions while neutral H_3 could coordinate with Zn^{2+} ions or hydrogen bond with O^{2-} ions. The adsorption of GT-16 on the $(10\bar{1}0)$ plane may occur *via* hydrogen bonding (neutral R_{12} with O^{2-}), electrostatic interactions (thiol and COO^- of C_{16} with Zn^{2+}, and M_5 sulfur atom lone pair with Zn^{2+}), and hydrophobic interactions (*via* the GGG-segment). Inferred from these differences, the presence of the GGGC-tag may have lowered the GT-16 density on the $(10\bar{1}0)$ plane due to a weaker hydrophobic adsorption contribution. In short, the calculation of adsorption energies and the prediction of binding moieties using a computational approach have provided a plausible explanation for the adsorption phenomenon observed.

Conclusions

A ZnO-BP (G-12) identified by Phage display methods and its -GGGC tagged derivative (GT-16) both affect ZnO crystal morphology in a concentration dependent fashion by altering the *c*-axis and *a*-axes growth rate of ZnO crystals. As a consequence, the aspect ratio of ZnO was reduced in their presence with the effect being more prominent in the presence of GT-16. For the first time, the amount of peptide adsorbed on different ZnO crystal planes has been quantified by a depletion method using ALD-grown oriented ZnO films. In conjunction with the confirmation of adsorption by XPS, this study has provided direct evidence for the modification of ZnO morphology *via* an adsorption–growth inhibition mechanism in the presence of ZnO-BP and its derivative. The correlation of peptide adsorption behavior with the alteration of crystal plane growth rates verified the preferential binding (discriminative behavior) of GT-16 on the (0001) plane over the $(10\bar{1}0)$ plane of ZnO crystals. Such behavior was not evident for G-12 which lacked the GGGC-tag, indicating that the GGGC-tag present in GT-16 was not essential for peptide adsorption on the (0001) plane of ZnO but provided GT-16 with plane selectivity characteristics. The calculated adsorption energies of G-12 and GT-16 on different ZnO planes were in broad agreement with the level of plane-selectivity shown experimentally. A prediction of binding moieties by a computational (MD) approach identified GGGC as being the cause of the plane selectivity behavior of GT-16.

The tuning of ZnO morphology *via* biomolecule adsorption is a complex phenomenon. The solution chemistry of amino acid residues, the nature of counterions, the surface chemistry of ZnO planes, and peptide sequences were all found to play a part and influenced the reaction. The total elucidation of this complex phenomenon would require further extensive studies. However, the results reported in this contribution provide evidence and insight into ZnO morphology-tuning, mediated by the adsorption of biomolecules on specific crystal plane(s) of ZnO crystals. The ultimate goal of these studies is to identify and understand the specific role(s) individual functionalities play within a given biomolecule in ZnO morphology tuning. By doing so, the specificity and multi-functionality of biomolecules in affecting ZnO morphology can be learnt and manipulated to tailor-make ZnO crystals with controllable morphology and properties.

Acknowledgements

This study was supported by funding from US Air Force Office of Scientific Research (AFOSR), FA9550-06-1-0154. We would like to thank Dr David J. Belton and Miss Clare Coveney for carrying out HPLC analysis and molecular weight analysis respectively on peptides studied. We would also like to convey our gratitude to Miss Emily Smith and Mr Ignacio Villar from the Department of Chemistry, University of Nottingham for performing the XPS analysis.

Notes and references

1 C. F. Klingshirn, *ChemPhysChem*, 2007, **8**, 782.
2 Z. L. Wang, *J. Phys.: Condens. Matter*, 2004, **16**, R829.
3 S. J. Pearton, D. P. Norton, K. Ip, Y. W. Heo and T. Steiner, *Prog. Mater. Sci.*, 2005, **50**, 293.
4 C. X. Xu, X. W. Sun, Z. L. Dong and M. B. Yu, *Appl. Phys. Lett.*, 2004, **85**, 3878.
5 L. Z. Wang, X. Y. Kong and J. M. Zuo, *Phys. Rev. Lett.*, 2003, **91**, 185502.
6 J. Y. Lao, J. Y. Huang, D. Z. Wang and Z. F. Ren, *Nano Lett.*, 2003, **3**, 235.
7 X. Y. Kong, Y. Ding, R. Yang and Z. L. Wang, *Science*, 2004, **303**, 1348.
8 Z. W. Pan, Z. R. Dai and Z. L. Wang, *Science*, 2001, **291**, 1947.
9 P. X. Gao and Z. L. Wang, *Science*, 2003, **125**, 11299.
10 X. Y. Kong and Z. L. Wang, *Nano Lett.*, 2003, **3**, 1625.
11 W. D. Yu, X. M. Li and X. D. Gao, *Appl. Phys. Lett.*, 2004, **84**, 2658.
12 Y. Yan, L. Zhou, Q. Xue and Y. Zhang, *J. Phys. D: Appl. Phys.*, 2008, **41**, 195402.
13 B. Cao and W. Cai, *J. Phys. Chem. C*, 2008, **112**, 680.
14 Y. Masuda, N. Kinoshita and K. Koumoto, *Electrochim. Acta*, 2007, **53**, 171.
15 R. Xie, D. Li, H. Zhang, D. Yang, M. Jiang, T. Sekiguchi, B. Liu and Y. Bando, *J. Phys. Chem. B*, 2006, **110**, 19147.
16 F. Lu, W. Cai and Y. Zhang, *Adv. Funct. Mater.*, 2008, **18**, 1047.
17 H. Imai, S. Iwai and S. Yamabi, *Chem. Lett.*, 2004, 768.
18 Z. R. Tian, J. A. Voigt, J. Liu, B. Mckenzie and M. J. Mcdermott, *J. Am. Chem. Soc.*, 2002, **124**, 12954.
19 J. Liang, J. Liu, Q. Xie, S. Bai, W. Yu and Y. Qian, *J. Phys. Chem. B*, 2005, **109**, 9463.
20 C.-L. Kuo, T.-J. Kuo and M. H. Huang, *J. Phys. Chem. B*, 2005, **109**, 20115.
21 T. Zhang, W. Dong, M. Keeter-Brewer, S. Konar, R. N. Njabon and Z. R. Tian, *J. Am. Chem. Soc.*, 2006, **128**, 10960.
22 M. Öner, J. Norwig, W. H. Meyer and G. Wegner, *Chem. Mater.*, 1998, **10**, 460.
23 A. Taubert, D. Palms, O. Weiss, T. Piccini and D. N. Batchelder, *Chem. Mater.*, 2002, **14**, 2594.
24 A. Taubert, G. Glasser and D. Palms, *Langmuir*, 2002, **18**, 4488.
25 G. Wegner, P. Baum, M. Müller, J. Norwig and K. Landfester, *Macromol. Symp.*, 2001, **175**, 349.
26 A. Taubert, C. Kubel and D. C. Martin, *J. Phys. Chem. B*, 2003, **107**, 2660.

27 R. C. Hoffmann, S. Jia, J. C. Bartolomé, T. M. Fuchs, J. Bill, P. C. J. Graat, and F. Aldinger, *J. Eur. Ceram. Soc.*, 2003, **23**, 2119.
28 R. C. Hoffmann, T. M. Fuchs, T. P. Niesen, J. Bill and F. Aldinger, *Surf. Interface Anal.*, 2002, **34**, 708.
29 Y. Peng, A.-W. Xu, B. Deng, M. Antonietti and H. Colfen, *J. Phys. Chem. B*, 2006, **110**, 2988.
30 J. Zhang, H. Liu, Z. Wang, N. Ming, Z. Li and A. S. Biris, *Adv. Funct. Mater.*, 2007, **17**, 3897.
31 L. Guo and S. Yang, *Chem. Mater.*, 2000, **12**, 2268.
32 N. Lepot, M. K. V. Bael, H. V. d. Rul, J. D'Haen, R. Peeters and F. D. Mullens, *Mater. Lett.*, 2007, **61**, 2624.
33 K. Biswas, B. Das and C. N. R. Rao, *J. Phys. Chem. C*, 2008, **112**, 2404.
34 J. Zhang, H. Liu, Z. Wang and N. Ming, *J. Cryst. Growth*, 2008, **310**, 2848.
35 M. Bitenc, M. Marinšek and Z. C. Orel, *J. Eur. Ceram. Soc.*, 2008, **28**, 2915.
36 R. Viswanatha and D. D. Sarma, *Chem.–Eur. J.*, 2006, **12**, 180.
37 D. Tao, W. Qian, Y. Huang and F. Wei, *J. Cryst. Growth*, 2004, **273**, 353.
38 L. Guo, J. X. Cheng, X.-Y. Li, Y. J. Yan, S. H. Yang, C. L. Yang, J. N. Wang and W. K. Ge, *Mater. Sci. Eng., C*, 2004, **16**, 123.
39 C. Pacholski, A. Kornowski and H. Weller, *Angew. Chem., Int. Ed.*, 2002, **41**, 1188.
40 R.-Q. Song, A.-W. Xu, B. Deng, Q. Li and G.-Y. Chen, *Adv. Funct. Mater.*, 2007, **17**, 296.
41 S. Musić, A. Šarić and S. Popović, *J. Alloys Compd.*, 2008, **448**, 277.
42 S. Lee, S. Jeong, D. Kim, B. K. Park and J. Moon, *Superlattices Microstruct.*, 2007, **42**, 361.
43 G. Begum, S. V. Manorama, S. Singh and R. K. Rana, *Chem.–Eur. J.*, 2008, **14**, 6421.
44 P. Gerstel, R. C. Hoffmann, P. Lipowsky, L. P. H. Jeurgens, J. Bill and F. Aldinger, *Chem. Mater.*, 2006, **18**, 179.
45 P. Gerstel, P. Lipowsky, O. Durupthy, R. C. Hoffmann, P. Bellina, J. Bill and F. Aldinger, *J. Ceram. Soc. Jpn.*, 2006, **114**, 911.
46 M. M. Tomczak, M. K. Gupta, L. F. Drummy, S. M. Rozenzhak and R. R. Naik, *Acta Biomater.*, 2009, **5**, 876.
47 R. d. l. Rica and H. Matsui, *Angew. Chem., Int. Ed.*, 2008, **47**, 5415.
48 Q. Wu, X. Chen, P. Zhang, Y. Han, X. C. Y. Yan and S. Li, *Cryst. Growth Des.*, 2008, **8**, 3010.
49 Q. Dong, H. Su, F. Song, D. Zhang and N. Wang, *J. Am. Ceram. Soc.*, 2007, **90**, 376.
50 L. P. Bauermann, A. d. Campo, J. Bill and F. Aldinger, *Chem. Mater.*, 2006, **18**, 2016.
51 Y.-H. Tseng, H.-Y. Lin, M.-H. Liu, Y.-F. Chen and C.-Y. Mou, *J. Phys. Chem. C*, 2009, **113**, 18053.
52 Q. Dong, H. Su, C. Zhang, D. Zhang, Q. Guo and F. Kiessling, *Chem. Eng. J.*, 2008, **137**, 428.
53 M. B. Dickerson, K. H. Sandhage and R. R. Naik, *Chem. Rev.*, 2008, **108**, 4935.
54 L. E. Greene, B. D. Yuhas, M. Law, D. Zitoun and P. Yang, *Inorg. Chem.*, 2006, **45**, 7535.
55 M. Jitianu and D. V. Goia, *J. Colloid Interface Sci.*, 2007, **309**, 78.
56 D. Yan, G. Yin, Z. Huang, M. Yang, X. Liao, Y. Kang, Y. Yao, B. Hao and D. Han, *J. Phys. Chem. B*, 2009, **113**, 6047.
57 Z. Huang, D. Yan, M. Yang, X. Liao, Y. Kang, G. Yin, Y. Yao and B. Hao, *J. Colloid Interface Sci.*, 2008, **325**, 356.
58 M. Umetsu, M. Mizuta, K. Tsumoto, S. Ohara, S. Takami, H. Watanabe, I. Kumagai and T. Adschiri, *Adv. Mater.*, 2005, **17**, 2571.
59 D. Weinzierl, D. Touraud, A. Lecker, A. Pfitzner and W. Kunz, *Mater. Res. Bull.*, 2008, **43**, 62.
60 S. V. Patwardhan, G. Patwardhan and C. C. Perry, *J. Mater. Chem.*, 2007, **17**, 2875.
61 M. Sarikaya, C. Tamerler, A. K.-Y. Jen, K. Schulten and F. Baneyx, *Nat. Mater.*, 2003, **2**, 577.
62 S. Brown, M. Sarikaya and E. Johnson, *J. Mol. Biol.*, 2000, **299**, 725.
63 S. Brown, *Nat. Biotechnol.*, 1997, **15**, 269.
64 S. Brown, *Nano Lett.*, 2001, **1**, 391.
65 R. R. Naik, S. J. Stringer, G. Agarwal, S. E. Jones and M. O. Stone, *Nat. Mater.*, 2002, **1**, 169.
66 C. K. Thai, H. Dai, M. S. R. Sastry, M. Sarikaya, D. T. Schwartz and F. Baneyx, *Biotechnol. Bioeng.*, 2004, **87**, 129.
67 K. Kjærgaard, J. K. Sørensen, M. A. Schembri and P. Klemm, *Appl. Environ. Microbiol.*, 2000, **66**, 10.
68 R. R. Naik, L. L. Brott, S. J. Clarson and M. O. Stone, *J. Nanosci. Nanotechnol.*, 2002, **2**, 95.
69 E. Eteshola, L. J. Brillson and S. C. Lee, *Biomol. Eng.*, 2005, **22**, 201.
70 H. Chen, X. Su, K.-G. Neoh and W.-S. Choe, *Langmuir*, 2008, **24**, 6852.
71 T. P. Chou, Q. Zhang, G. E. Fryxell and G. Cao, *Adv. Mater.*, 2007, **19**, 2588.
72 H. Bai, F. Xu, L. Anjia and H. Matsui, *Soft Matter*, 2009, **5**, 966.
73 N. Yokoo, T. Togashi, M. Umetsu, K. Tsumoto, T. Hattori, T. Nakanishi, S. Ohara, S. Takami, T. Naka, H. Abe, I. Kumagai and T. Adschiri, *J. Phys. Chem. B*, 2010, **114**, 480.
74 L. Shi, J. Zhou and S. Gunasekaran, *Mater. Lett.*, 2008, **62**, 4383.
75 Z. R. Tian, J. A. Voigt, J. Liu, B. Mckenzie, M. J. Mcdermott, M. A. Rodriguez, H. Konishi and H. Xu, *Nat. Mater.*, 2003, **2**, 821.
76 B. Liu and H. C. Zeng, *J. Am. Chem. Soc.*, 2003, **125**, 4430.
77 B. Liu and H. C. Zeng, *Langmuir*, 2004, **20**, 4196.
78 M. Muthukumar, *J. Chem. Phys.*, 2009, **130**, 161101.
79 Y. K. Gao, F. Traeger, O. Shekhah, H. Idriss and C. Wöll, *J. Colloid Interface Sci.*, 2009, **338**, 16.
80 S. Irrera, D. Costa and P. Marcus, *J. Mol. Struct.*, 2009, **903**, 49.
81 G. Mandal, S. Bhattacharya and T. Ganguly, *Chem. Phys. Lett.*, 2009, **472**, 128.
82 M. Bardhan, G. Mandal and T. Ganguly, *J. Appl. Phys.*, 2009, **106**, 034701.
83 Z. J. Deng, G. Mortimer, T. Schiller, A. Musumeci, D. Martin and R. F. Minchin, *Nanotechnology*, 2009, **20**, 455101.
84 W. C. Chan and P. D. White, *Fmoc Solid Phase Peptide Synthesis*, Oxford university Press, New York, 2000.
85 S.-Y. Pung, K.-L. Choy, X. Hou and C. Shan, *Nanotechnology*, 2008, **19**, 435609.
86 C. H. Liu, M. Yan, X. Liu, E. Seelig and R. P. H. Chang, *Chem. Phys. Lett.*, 2002, **355**, 43.
87 GROMACS is a free software available under the GNU General Public License.
88 N. Metropolis, A. W. Rosenbluth, M. N. Rosenbluth, A. H. Teller and E. Teller, *J. Chem. Phys.*, 1953, **21**, 1087.
89 Z. Zhang, M. Lu, H. Xu and W.-S. Chin, *Chem.–Eur. J.*, 2007, **13**, 632.
90 Q. Li, V. Kumar, Y. Li, H. Zhang, T. J. Marks and R. P. H. Chang, *Chem. Mater.*, 2005, **17**, 1001.
91 S.-C. Liou, C.-S. Hsiao and S.-Y. Chen, *J. Cryst. Growth*, 2005, **274**, 438.
92 A. Sugunan, H. C. Warad, M. Boman and J. Dutta, *J. Sol-Gel Sci. Technol.*, 2006, **39**, 49.
93 H. Wang, C. Xie, D. Zeng and Z. Yang, *J. Colloid Interface Sci.*, 2006, **297**, 570.
94 S. Aisawa, E. Ishida, S. Takahashi, H. Hirahara and E. Narita, *Chem. Lett.*, 2005, 630.
95 S. Aisawa, S. Takahashi, W. Ogasawara, Y. Umetsu and E. Narita, *J. Solid State Chem.*, 2001, **162**, 52.
96 A. Barth, *Prog. Biophys. Mol. Biol.*, 2000, **74**, 141.
97 O. Deschaume, A. Fournier, K. Shafran and C. C. Perry, *New J. Chem.*, 2008, **32**, 1346.
98 K. Gorna, R. Muñoz-Espí, F. Gröhn and G. Wegner, *Macromol. Biosci.*, 2007, **7**, 163.
99 Y.-S. Fu, X.-W. Du, J. Sun, Y.-F. Song and J. Liu, *J. Alloys Compd.*, 2008, **461**, 527.
100 I. Bertini, H. B. Gray, E. I. Stiefel and J. S. Valentine, *Biological Inorganic Chemistry: Structure and Reactivity*, University Science Book, California, 2007.
101 U. Brand, M. Rombach, J. Seebacher and H. Vahrenkamp, *Inorg. Chem.*, 2001, **40**, 6151.